Supporting information

Structural Variety in Iridate Oxides and Hydroxides From Hydrothermal Synthesis

Kripasindhu Sardar, Janet Fisher, David Thompsett, Martin R. Lees, Guy J. Clarkson, Jeremy Sloan, Reza J. Kashtiban and Richard I. Walton

S1: Further Experimental Details

Powder X-ray diffraction patterns were measured using a Bruker D8 Advance X-ray diffractometer operating with Cu Kα radiation and equipped with a VÅNTEC-1 solid-state detector. The diffractometer was fitted with an Anton-Parr XRK900 chemical reaction chamber to allow measurements to be made as a function of temperature and gas environment.

D.C. magnetisation measurements were carried out using a Quantum Design Magnetic Property Measurement System (MPMS) squid magnetometer. The powdered samples were placed in a gel capsules and mounted in plastic straws.

Infra-red spectra were recorded using a Perkin Elmer Paragon 1000 FT-IR Spectrometer in attenuated total reflection mode. Thermogravimetric analysis (TGA) and differential thermal analysis (DTA) was performed with a heating rate of 10 ^{o}C min^{-1} in air using a Mettler-Toledo instrument.

HRTEM information: specimens were examined using a 300 kV Field Emission Gun High Resolution Transmission Electron Micro scope (JEOL JEM-3000F, Cs = 0.57 mm, point resolution = 0.16 nm). Lattice images and electron diffraction patterns were obtained from individually aligned crystallites mounted on a 6nm thin amorphous carbon support film (Agar) at a magnification of x 600,000. Unprocessed images were acquired on a Gatan model 794 (1024 x 1024 pixel) CCD camera for which the magnification was calibrated with MgO [111] lattice spacings. Image simulations were carried out using the multislice algorithm using parameters typical for this instrument (Cs = 0.57 mm, accelerating voltage 300 kV). The scanning electron microscope (SEM) images of the strontium iridate sample were recorded using Zeiss SUPRA 55VP FEG scanning electron microscope.

Powder diffraction data were analysed using the GSAS suite of software.[1]

Elemental analysis for metals was performed by Medac Ltd UK using ICP-MES for Na, Ca, Sr and Ir after digestion in 5 M HBr. The analysis for fluorine was performed by Schöniger flask combustion followed by titration for fluorine, also by Medac Ltd.

S2: $Sr_2Ir(OH)_8$

S2.1 Synthesis

Stoichiometric amounts of $Sr(NO_3)_2$ (anhydrous, 99% Across organics) and $IrCl_3.5H_2O$ (0.25 mmol, Alfa Aesar: water content verified using TGA) were weighed as solids in a 20 ml Teflon liner to which 2.5 ml of distilled water and 5 ml ~12 M aqueous NaOH. The mixture was stirred for 3 hours before being sealed in a stainless steel autoclave and placed inside a pre-heated oven at 195 ^oC where it was maintained for 9 days. The crystalline solid was isolated by suction filtration and washed with hot water before being dried at 80 ^oC before further study. Reactions performed at 240 ^oC gave a black polycrystalline impurity, identified as nanocrystalline iridium metal by powder XRD.

S2.2 Single Crystal X-ray Diffraction

A single crystal was selected for single crystal structure analysis: green block of 0.40 x 0.08 x 0.03 mm^3. The crystal was glued to a glass fibre and the data recorded at 296(2) K using a Oxford Diffraction Gemini four-circle system with Ruby CCD area detector. Maximum theta was 29.07 deg and the *hkl* ranges were -8/ 7, -14/ 11, -8/ 6. 1848 reflections measured with 844 unique [R(int) = 0.0248]. Absorption correction was by semi-empirical from equivalents; minimum and maximum transmission factors: 0.21; 1.00. No crystal decay was observed. The structure was solved by direct methods using SHELXS[2] with hydrogen atoms located in a Fourier difference map and refined with a distance restraint. Anisotropic displacement parameters were used for all non-H atoms; H-atoms were given isotropic displacement parameters equal to 1.5 times the equivalent isotropic displacement parameter of the atom to which the H-atom is attached.

Goodness-of-fit on F^2 was 1.015, R1[for 729 reflections with I>2sigma(I)] = 0.0234, wR2 = 0.0546. Data / restraints / parameters 844/ 4/ 65. Extinction coefficient 0.0175(8). Largest difference Fourier peak and hole 1.658 and -1.804 e A^{-3} .

Space group: *P*2/*n* a = 5.9657(3) Å, b = 10.9919(4) Å, c = 6.0097(3) Å, β = 112.903(6)

Table S2.1. Atomic coordinates (× 10^4) and equivalent isotropic displacement parameters (Å^2 × 10^3) for $Sr_2Ir(OH)_8$. *U*(eq) is defined as one third of the trace of the orthogonalised U_{ij} tensor.

	x	y	z	*U*(eq)
Ir(1)	0	0	0	6(1)
Sr(1)	2735.9(11)	3724.2(5)	1048.9(9)	9(1)
O(1)	195(9)	1686(4)	-1256(7)	10(1)
O(2)	-1163(9)	620(3)	2495(7)	9(1)
O(3)	3458(9)	250(4)	2378(8)	11(1)
O(4)	5540(9)	2289(4)	196(7)	15(1)
H1	-0.120(6)	0.199(6)	-0.176(12)	-
H2	-0.225(11)	0.112(6)	0.173(11)	-
H3	0.422(13)	0.073(5)	0.183(13)	-
H4	0.633(13)	0.265(6)	-0.052(12)	-

Hydrogens H1-H4 are attached to oxygens O1-O4, respectively.

Bond valence sums[3] were performed to confirm the valence of each atom (note hydrogen atoms were note included):

Ir: 4.07 **Sr:** 2.05 **O1:** 1.08 **O2:** 1.29 **O3:** 1.12 **O4**: 0.6

This confirms that each oxygen atom is part of a hydroxide group.

S2.3 Powder X-ray Diffraction

Figure S2.1 shows observed data along with the pattern calculated from the single crystal structure. Note effects of preferred orientation due to anisotropic crystal shape.

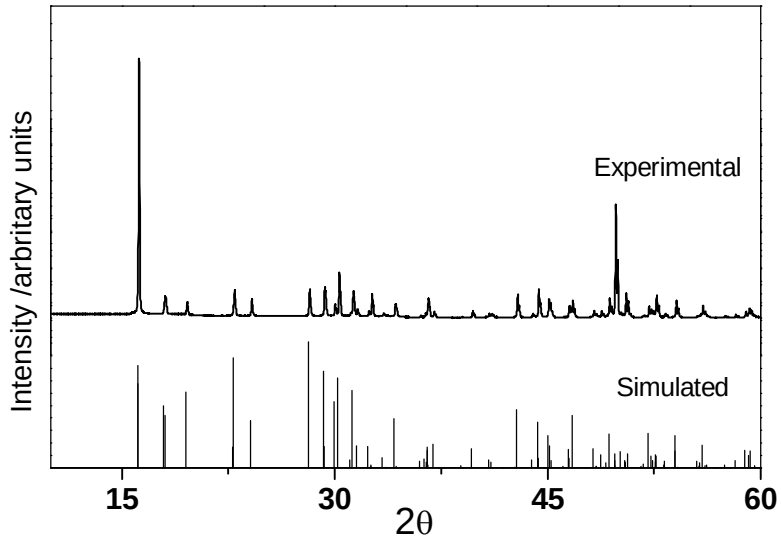

Figure S2.1: Observed and calculated powder XRD patterns for $Sr_2Ir(OH)_8$

S2.4: Thermogravimetric Analysis

TGA in air shows a sharp mass loss of 7-8% around 290 ^oC, while DTA shows an endothermic peak at 290 ^oC with an onset around 256 ^oC. This weight loss is equivalent to release of two H_2O molecules, attributed to dehydroxylation of $Sr_2Ir(OH)_8$ to produce '$Sr_2IrO_4.2H_2O$' (expected 7.15 %), although the material formed at this point is amorphous (see below). TGA also confirms the absence of any crystal water, since only small mass loss (<1 %) occurs before 290 ^oC, ascribed to surface water (also *cf.* $BaIr(OH)_6.H_2O$ described below).

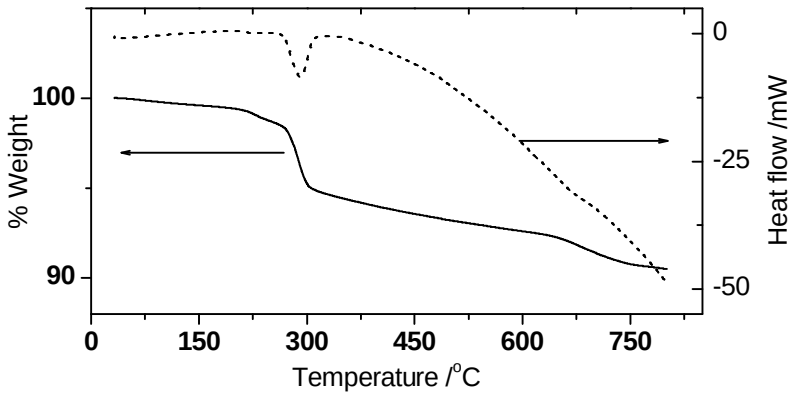

Figure S2.2: TGA/DTA trace of $Sr_2Ir(OH)_8$

S2.5 Thermodiffractometry

In situ XRD of $Sr_2Ir(OH)_8$ while heating to 550 ^oC is shown in Figure S1.3. The XRD patterns recorded from 30- 270 ^oC show the presence of pure $Sr_2Ir(OH)_8$. The intensities of XRD peaks are drastically reduced at 290 ^oC and the XRD pattern recorded at 310 ^oC clearly demonstrates that the first decomposition product of $Sr_2Ir(OH)_8$ is an amorphous phase. Very broad peaks of $SrCO_3$ and Ir metal can be identified in the XRD pattern at 350 ^oC and these peaks become sharper upon further heating up to 550 ^oC.

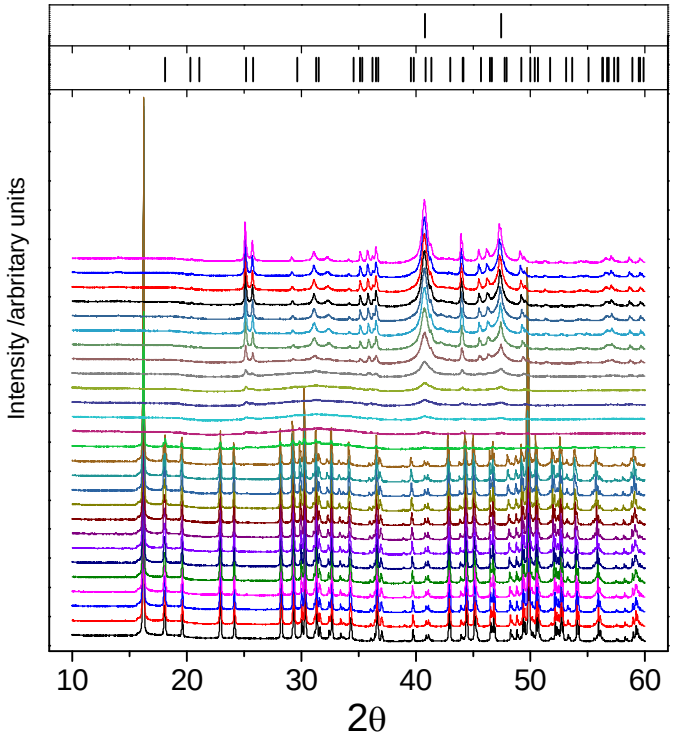

Figure S2.3: Powder XRD patterns from $Sr_2Ir(OH)_8$ recorded during *in situ* heating in air from 30-550 ^oC. Patterns were recorded at temperature intervals of 20 ^oC. All patterns are offset along the y axis for clarity. Upper and lower panels, showBragg peak positions for Ir (ICSD #659854) and $SrCO_3$ (ICSD #160088), respectively

S2.6 Magnetisation

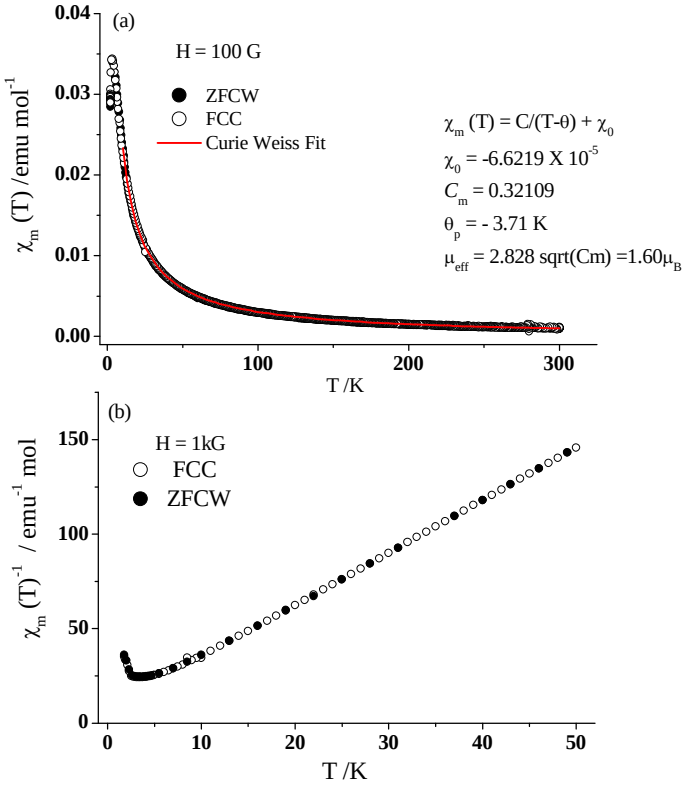

Figure S2.4: Magnetisation curves of $Sr_2Ir(OH)_8$ showing (a) the variation of susceptibility in the temperature region 2-300 K including a Curie Weiss fit to the data above the temperature where the anomaly was seen in low-temperature region and (b) the inverse susceptibility versus temperature

S3: $Ca_2IrF(OH)_6.OH$

S3.1 Synthesis

Stoichiometric amounts of $Ca(NO_3)_2.4H_2O$ (99%, Lancaster) and $IrCl_3.5H_2O$ (0.3 mmol, Alfa Aesar; water content verified using TGA) were weighed as solids in a 20 ml Teflon liner. To this mixture, 11.5 mmol of solid NaOH was added, followed by 8 ml of deionised water. The mixture was stirred for 30 minutes and than 1 molar equivalent (per Ir) of solid NaF was added with further stirring before the Teflon liner was sealed in a stainless steel autoclave and placed inside a pre-heated oven at 240 ^oC where it was maintained for 72 hours. The crystalline solid was isolated by suction filtration and washed with hot water before being dried at 80 ^oC before further study.

S3.2 Single Crystal X-ray Diffraction

A yellow, needle-shaped single crystal (0.20 x 0.02 x 0.02 mm^3) was selected for analysis and mounted on a glass fibre and data recorded at 296(2) K using a Oxford Diffraction Gemini four-circle system with Ruby CCD area detector. Maximum theta was 29.12 deg. *hkl* ranges were -10/ 14, -14/ 9, -7/ 5. 2757 reflections were measured of which 429 unique [R(int) = 0.0303]. Absorption correction by semi-empirical from equivalents; minimum and maximum transmission factors: 0.51; 1.00. Systematic absences indicated space group $P4_2/ncm$ and shown to be correct by successful refinement. No crystal decay was observed. The structure was solved by direct methods using SHELXS[2] with additional light atoms found by Fourier methods. Hydrogen atoms were located in a difference map. As the O1-H1 and O2-H2 distances had slightly different values but very similar chemical environments they were refined with a DFIX instruction (DFIX 0.85) to ensure consistency. The O3-H3 was subsequently set to be the same length. Anisotropic displacement parameters were used for all non-H atoms; H-atoms were given isotropic displacement parameter equal to 1.5 times the equivalent isotropic displacement parameter of the oxygen to which they are attached.

Goodness-of-fit on F^2 was 0.889, R1[for 275 reflections with I>2sigma(I)] = 0.0183, wR2 = 0.0455. Data / restraints / parameters 429/ 3/ 37. Largest difference Fourier peak and hole 0.728 and -1.310 $e.A^{-3}$.

Space group: $P4_2/ncm$ a = 10.6331(4) Å, b = 10.6331(4) Å, c = 5.6597(3) Å

Table S3.1. Atomic coordinates (× 10^4) and equivalent isotropic displacement parameters (Å^2 × 10^3) for $Ca_2IrF(OH)_6.OH$. *U*(eq) is defined as one third of the trace of the orthogonalised U_{ij} tensor.

	x	y	z	U(eq)
Ir(1)	5000	10000	5000	5(1)
Ca(1)	3708.4(8)	8708.4(8)	0	8(1)
F(1)	2500	7500	2500	9(1)
O(1)	4874(3)	8256(3)	3681(5)	9(1)
O(2)	5634(3)	9366(3)	8101(6)	8(1)
O(3)	7500	7500	2754(9)	19(2)
H(1)	5594(19)	8000(40)	3280(70)	-
H(2)	0.6199(7)	0.8801(7)	0.801(10)	-
H(3)	7500	7500	1250(40)	-

Bond valence sums[3] were performed to confirm the valence of each atom (note hydrogen atoms are not included, and O3 the isolated hydroxide anion, held by hydrogen bonding was not considered):

Ir: 4.19 **Ca:** 2.11 **O1:** 1.16 **O2:** 1.30 **F1:** 1.15

F1 was clearly a fluorine atom by consideration of its temperature factor: if set as an oxygen an unreasonable *U*(eq) value was obtained and a considerably higher goodness of fit.

This confirms that the two framework oxygen atoms are hydroxide ions.

The 'extra-framework' atom (O3) could be refined as either a fluoride or a hydroxide, with the latter giving a a slightly better fit.

(i) Refined as a fluoride R1 = 0.0188 for 275 Fo > 4sig(Fo) 0.0381 for all 429 data WGHT 0.0283 wR2 = 0.0478, GooF = S = 0.908, highest Q peak Q1 0.75

(ii) Refined as an oxygen R1 = 0.0184 for 275 Fo > 4sig(Fo) 0.0372 for all 429 data WGHT 0.0284 wR2 = 0.0477, GooF = S = 0.906, highest Q peak Q1 0.71

However, the distance between these atoms is 2.8298(1) Å, which indicates the presence of hydrogen bonding interactions parallel to the channels along {001}.

Bulk elemental analysis (ICP) shows 4.6 % F, 22.3 % Ca and 40.0 % Ir in good agreement the expected values of 4.6 % F, 19.5 % Ca and 46.9 % Ir for $Ca_2IrF(OH)_6.OH$.

S3.3 Powder X-ray Diffraction

Figure S3.1 shows observed data along with the pattern calculated from the single crystal structure. Note effects of preferred orientation due to anisotropic crystal shape.

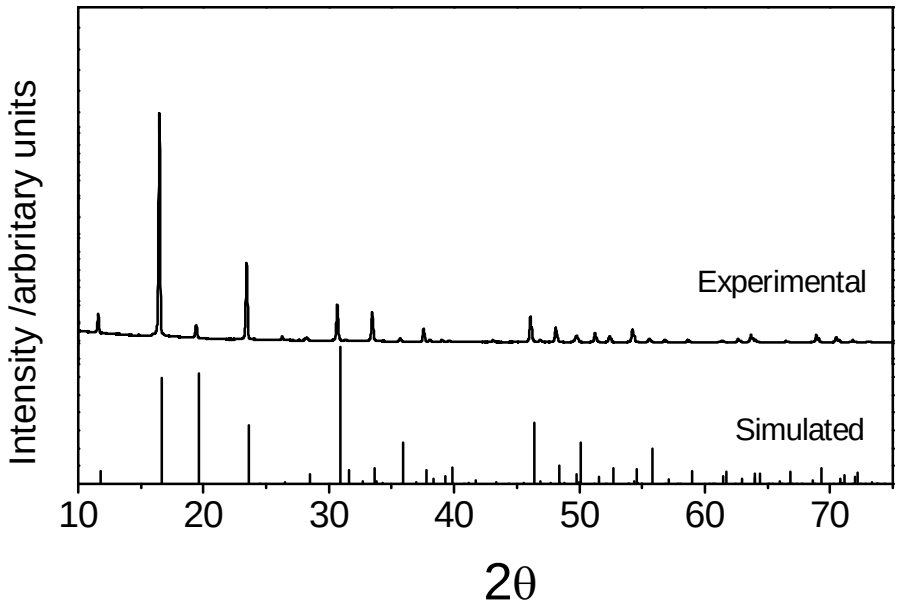

Figure S3.1: Observed and calculated powder XRD patterns for $Ca_2IrF(OH)_6OH$

S3.4: Thermogravimetric Analysis

TGA suggests the absence of any crystal water by comparison to $Sr_2Ir(OH)_8$ described above (and also in comparison to $BaIr(OH)_6.H_2O$ described below) with only a neglible mass loss up to just above 300 ^oC, at which point an abrupt dehydroxylatation occurs. (See below.)

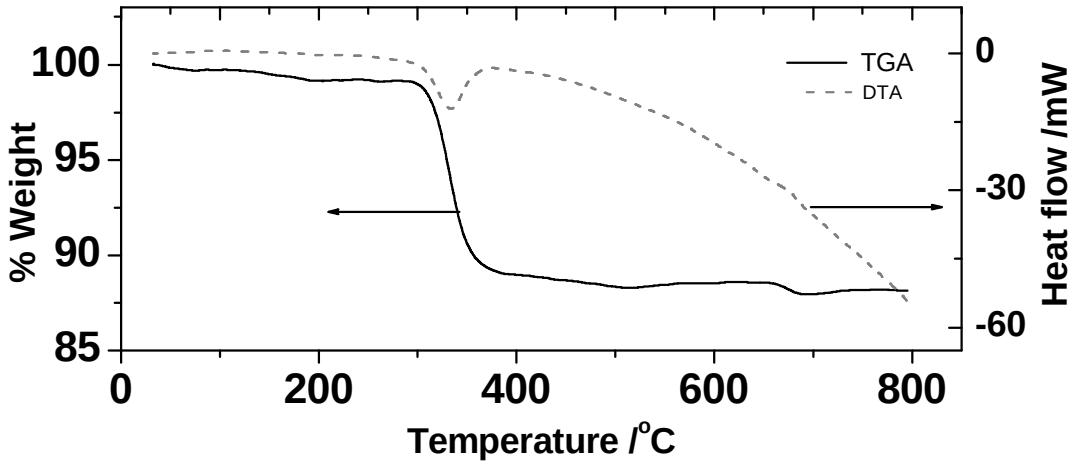

Figure S3.2: TGA/DTA trace of $Ca_2IrF(OH)_6OH$

S3.5 Thermodiffractometry

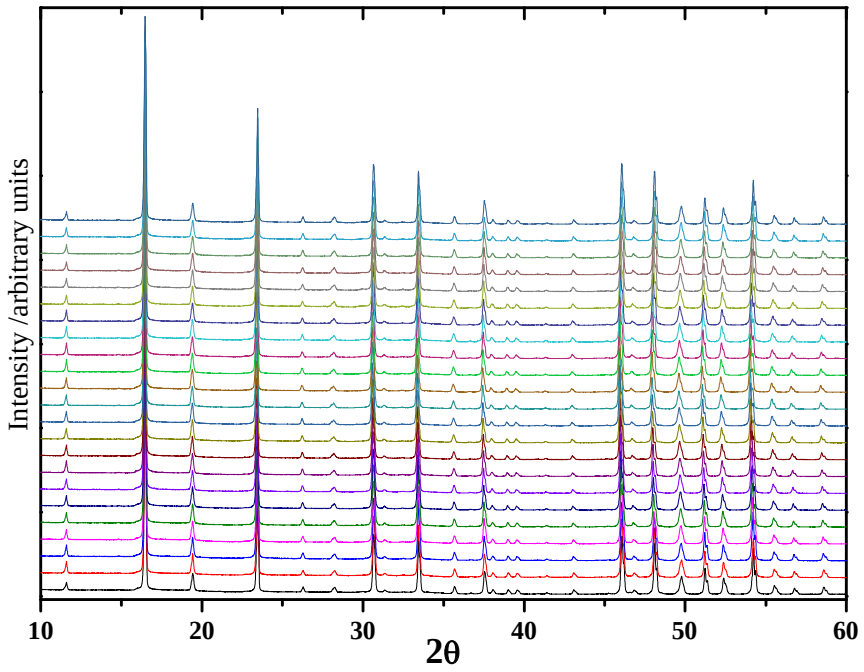

Figure S3.3: *In situ* XRD heating of $Ca_2IrF(OH)_6OH$ over 30-250-30 ^oC showing thermal stability up to 250 ^oC

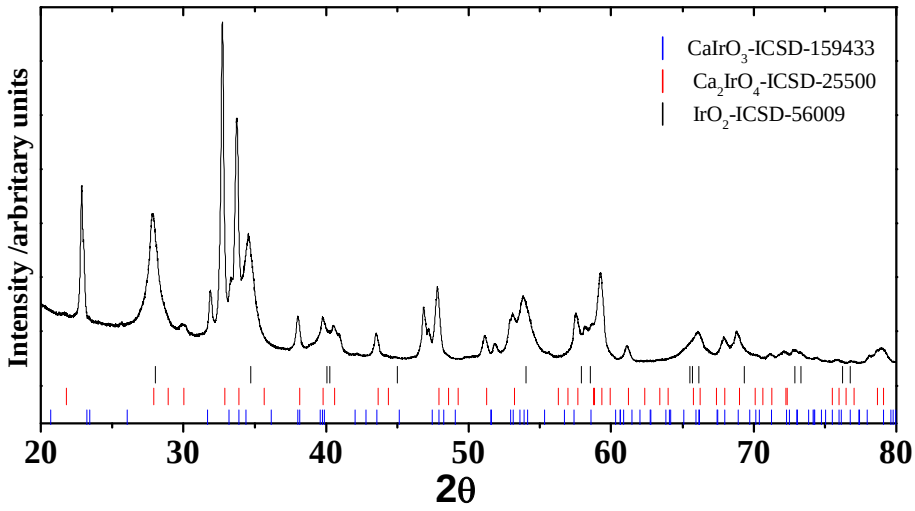

Figure S3.4: PXRD pattern of the sample heated at 800 ^oC for 6 hours showing formation of mixture of Ca_2IrO_4, $CaIrO_3$ and IrO_2

S3.6 Magnetisation

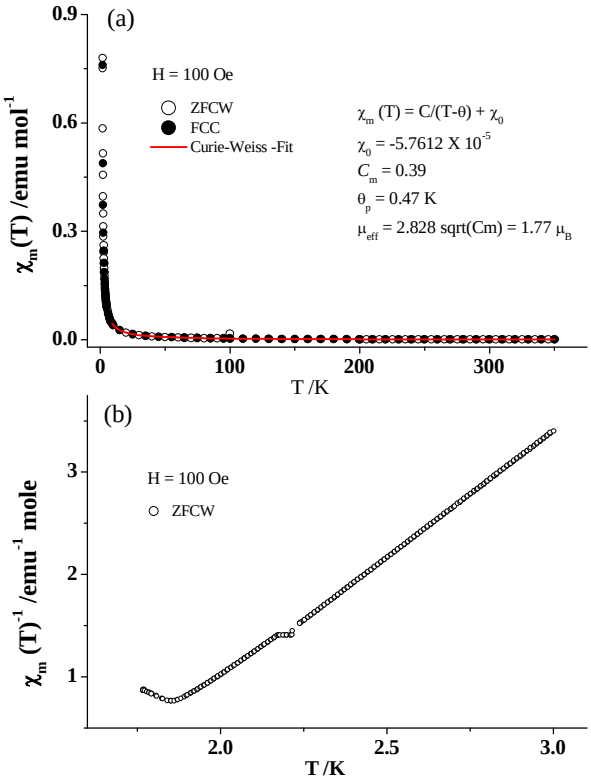

Figure S3.5 (a) Molar magnetic susceptibility as a function of temperature for 2-350 K, (b) inverse susceptibility versus temperature including a Curie Weiss fit to the data above the temperature where the anomaly was seen in low-temperature region (10 – 350 K).

S4: $BaIr(OH)_6.H_2O$

S4.1 Synthesis

Stoichiometric amounts of $Ba(NO_3)_2$ (anhydrous, 99.999%, Aldrich) and and $IrCl_3.5H_2O$ (based on 0.25 mmol of Ir), Alfa Aesar, water content verified using TGA) were weighed as solids in a 20 ml Teflon liner. To this mixture, 3 ml deionised water was added and the mixture was stirred for 10 minutes. To this mixture 5 ml 12 M NaOH solution was added and continued stirring for 2 h before the Teflon liner was sealed in a stainless steel autoclave and placed inside a pre-heated oven at 80 ^oC where it was maintained for 9 days. A bluish solid was isolated by suction filtration and washed with hot water before being dried at 80 ^oC before further study.

S4.2 Powder X-ray Diffraction

No suitable single crystals of $BaIr(OH)_6.H_2O$ were formed for structure analysis, hence the powder X-ray diffraction data were analysed using the published structrue of $BaPt(OH)_6.H_2O$ as a starting model.[4] Figure S4.1 shows a final profile fit (Le Bail fitting method).

$P\,2_1/m$ a = 6.27814(13) Å b = 6.24045(19) Å c = 8.64608(11) Å β = 107.9125(20)

wR_p = 0.0473 R_p = 0.0318 χ^2 = 9.467

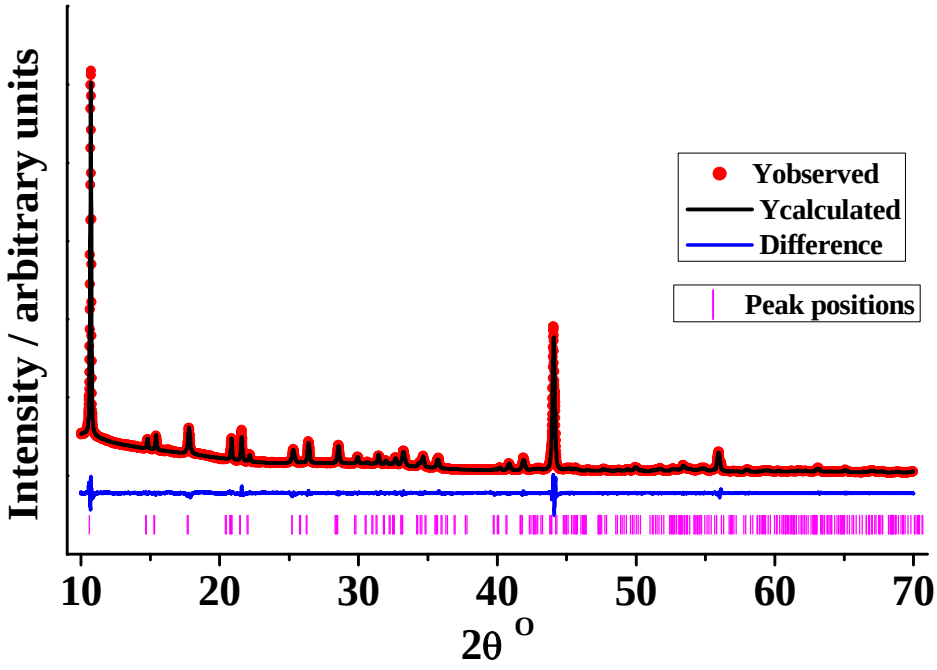

Figure S4.1: Final Le Bail profile fit for $BaIr(OH)_6.H_2O$

S4.2: Thermogravimetric Analysis

TGA shows a gradual mass loss at the start of heating to 150 ^{o}C which is consistent with the loss of crystal water (observed 4.2 %, expected 4.0 %) to yield $BaIr(OH)_{6.}$ This is then followed by subsequent mass losses correspond to dehydroxylation to yield hexagonal $BaIrO_3$, as shown by powder XRD, Figure S4.3.

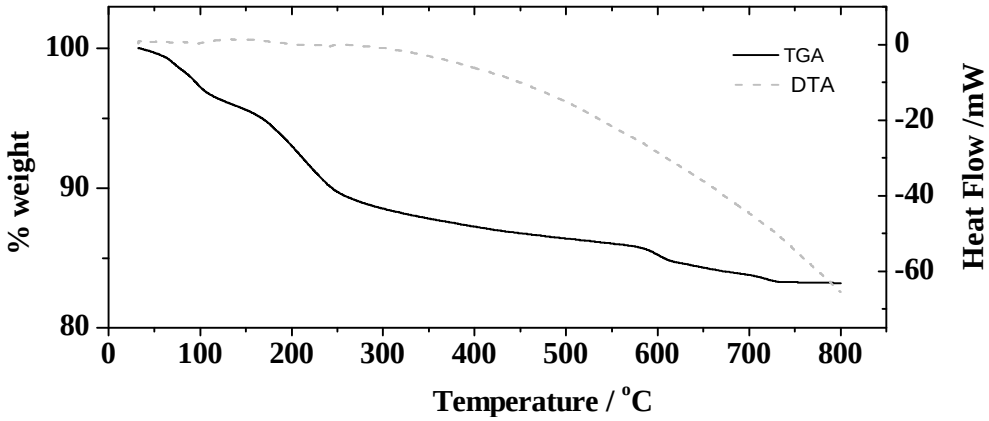

Figure S4.2: TGA/DTA trace of $BaIr(OH)_6$ H_2O

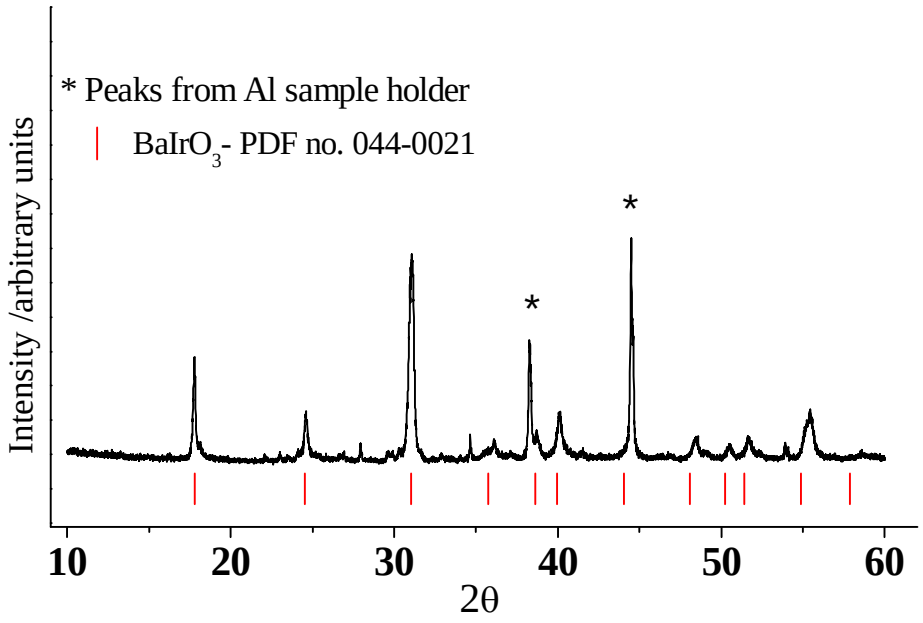

Figure S4.3: Powder XRD pattern of the thermally decomposed $BaIr(OH)_6.H_2O$ (800 ^{o}C in air for 3 hours)

S4.3: Magnetisation

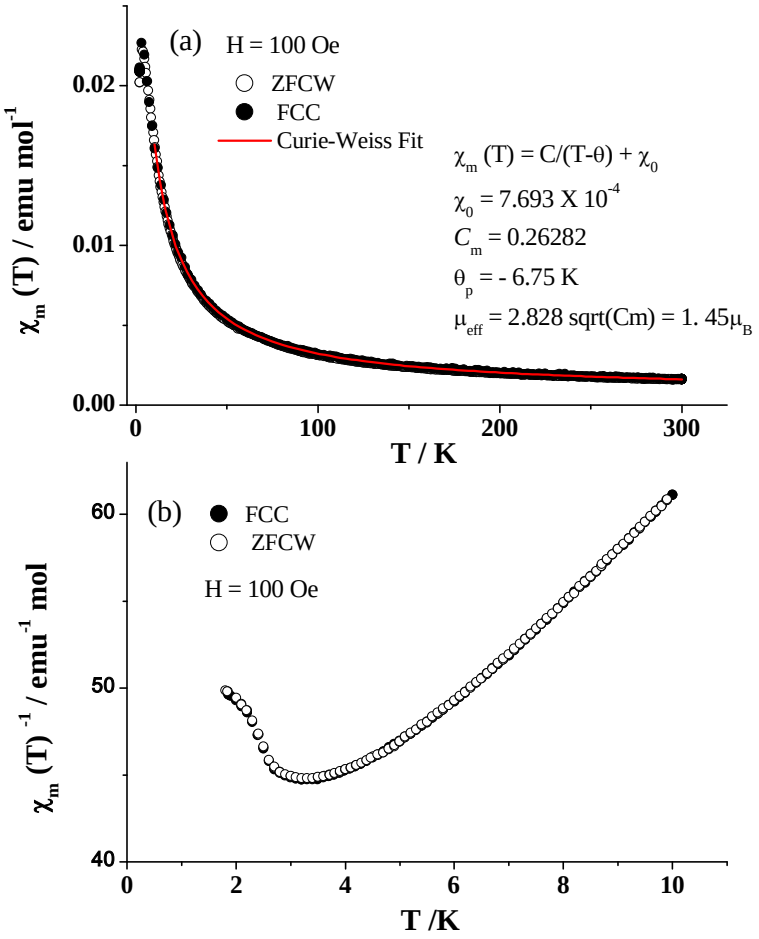

S4.4 Magnetisation curves of $BaIr(OH)_6.H_2O$ showing (a) the variation of susceptibility in the 2-300 K temperature region and (b) the inverse susceptibility versus temperature including a Curie Weiss fit to the data at temperatures above 7 K.

S5: IR analysis of the iridate hydroxides

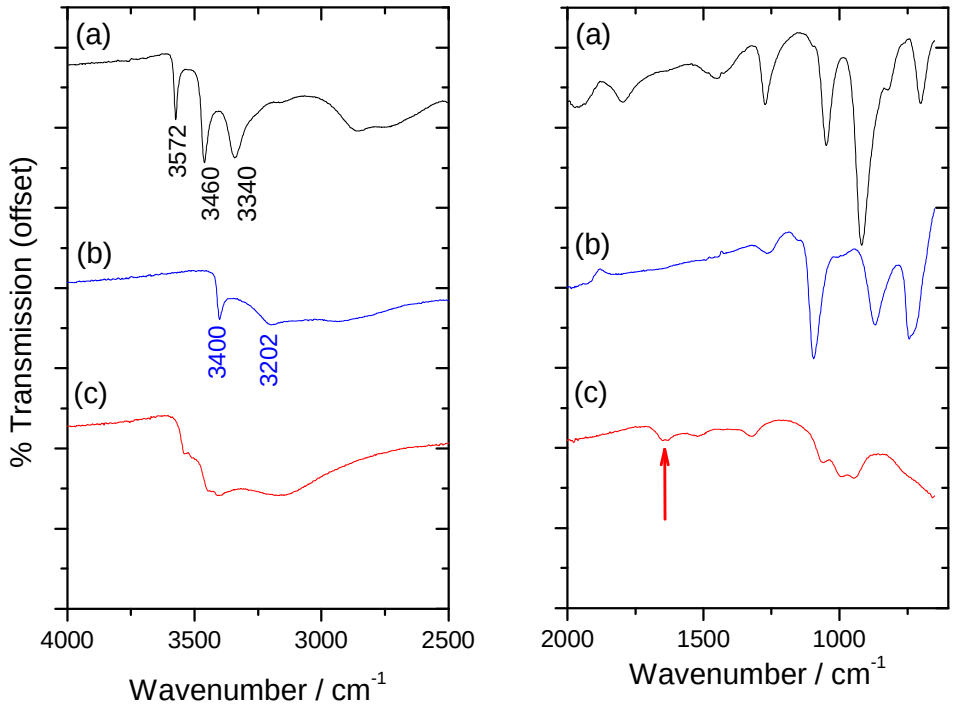

Figure S5.1: IR Spectra of (a) $Sr_2Ir(OH)_8$ (b) $CaIrF(OH)_6.OH$ and (c) $BaIr(OH)_6.H_2O$ The H-O-H bend of crystal water is indicated by an arrow in (c).

The IR spectrum of $Sr_2Ir(OH)_8$ shows three sharp well-resolved peaks in the O-H stretching region as labelled on Figure S5.1a. This is consistent with the presence of four crystallographic OH groups, three of which bridge two Sr centres and one Ir, and the fourth bridges just two strontiums, and is similar to the published IR spectrum of the related material $Sr_2Sn(OH)_8$.[5] Other important features may be assigned: 1270 cm^{-1} = δ(MOH); 1047 = δ(M-OH-M) and 922 & 704 cm^{-1} = ν(MO). In the case of $CaIrF(OH)_6.OH$ only two peaks are seen in the O-H stretching region and these may be assigned as arising from two OH environments: the type bridging two Ca and one Ir centres (3400 cm^{-1}) and the infinite hydrogen bonded chains of OH (at 3202 cm^{-1}); the second is disinctly different from the first type or those seem in the strontium material. Peaks seen for $CaIrF(OH)_6.OH$ in the region 1300 – 500 cm^{-1} are similar to those seen in the strontium iridium hydroxide. In the case of $BaIr(OH)_6.H_2O$ the peaks in the O-H stretching regio are broad, but this is consistent with spectra measured from the material $BaSb(OH)_6.2H_2O$.[6] Importantly we observe the H-O-H bend of crystal water at ~1628 cm^{-1} (*cf.* 1630 cm^{-1} in $BaSb(OH)_6.2H_2O$[6]), and this is absent in the strontium and calcium materials.

S6: $Na_{0.8}Sr_{2.2}Ir_3O_{10.1}$

S6.1: Synthesis

A 3:4 molar ratio of $Sr(NO_3)_2$ and $IrCl_3.5H_2O$, based on 0.2 mmol of Ir, was mixed with 20 mmol of solid NaOH in 3 ml deionised water within a 20 ml Teflon cup and stirred for ten minutes. To this was added 10 µl of HF (40 % in water) followed by stirring for a further hour and then the addition of 6 ml of H_2O_2 (27% Alfa Aesar) dropwise whilst stirring. The homogeneous mixture was sealed in a stainless-steel autoclave and placed in pre-heated overn at 240 ^oC for a period of 72 hours. The black solid product was isolated by suction filtration after cooling and thoroughly washed with deionised water followed and then dried at 80 ^oC in air before further study.

S6.2 Structure refinement.

Laboratory powder XRD revealed a $KSbO_3$-type structure with all Bragg refelection indexed on a primitive cubic unit cell (a ~ 9.45 Å) with no systematic absences expected for the body-centred variant of the structure, Figure S6.1. Powder neutron diffraction data were measured on the POLARIS diffractoneter at ISIS, the UK neutron source. The known structure of $La_3Ir_3O_{11}$[7] was used as a starting point for refinement with data from Bank C. Since elemental analysis confirmed the presence of sodium in the material, partial occupancy of the 8e site was refined.We have also examined the refinement of NPD data by incorporation of Na in 4 b site, however, the fitting worsens with unrealistic U_{iso} and occupancy values. The situation here is similar to that in $K_{0.1}Li_{0.9}SbO_3$, where K occupies only the 8e site of the $KSbO_3$ type structure.[8] The final crystal structure parameters are shown in Table S4.1, giving a refined composition $Na_{0.8}Sr_{2.2}Ir_3O_{10.1}$.

Bulk analysis (ICP analysis, following digestion using HBr) for metals gave the following results:

F < 0.03 % Ir 53.92 % Na 1.91 % Sr 18.42 %

In excellent agreement with expected values for $Na_{0.8}Sr_{2.2}Ir_3O_{10.1}$:

F 0.00 Ir 48.86 % Na 2.12 % Sr 18.66 %

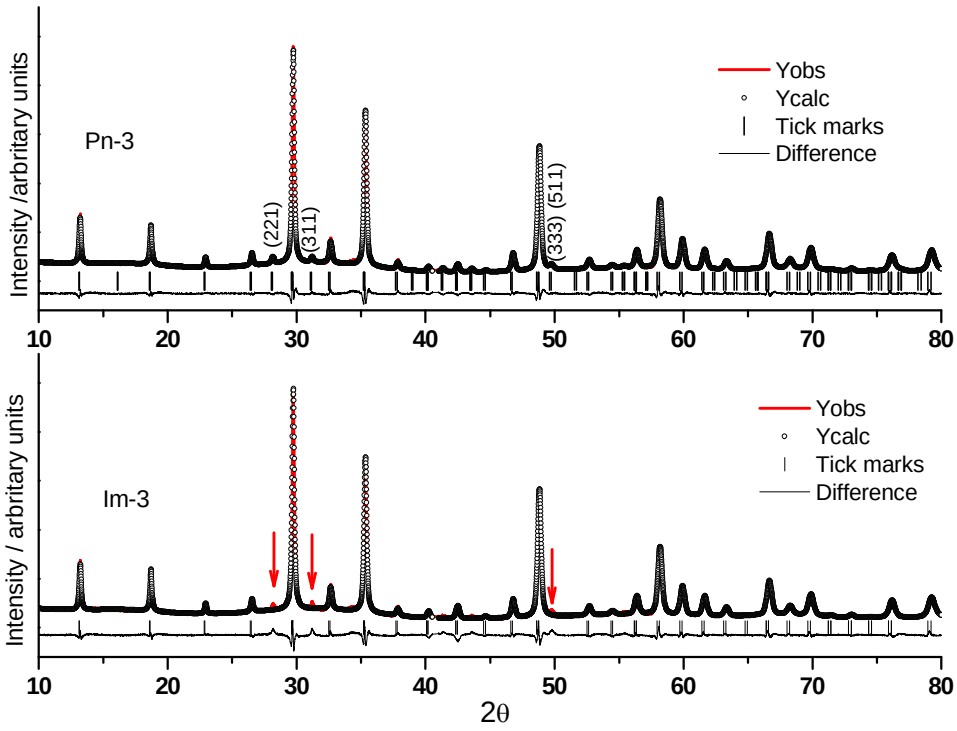

Figure S6.1: Le-bail profile refinement of powder XRD pattern in Pn-3 and Im-3 space groups showing presence of h+k+l = 2n reflections which are not allowed in body centered lattice.

Table S6.1: Refinement of powder neutron diffraction data for $Na_{0.8}Sr_{2.2}Ir_3O_{10.1}$

Space group $Pn\bar{3}$, a = 9.45688(22) Å, V = 845.753(34) Å^3

Atom Site	**Wyck.**	**S.O.F.**	**x**	**y**	**z**	**U [Å^2] × 100**
Ir1	12g	1	0.59285(16)	3/4	1/4	0.358(6)
Sr1	4b	1	0	0	0	8.88(52)
Sr2	8e	0.578(26)	0.40055(30)	0.40055(30)	0.40055(30)	1.32(8)
Na1	8e	0.422(26)	0.40055(30)	0.40055(30)	0.40055(30)	1.32(8)
O1	12f	1	0.61315(33)	1/4	1/4	0.941(44)
O2	24h	1	0.25918(25)	0.58980(17)	0.54434(18)	0.313(12
O3	8e	0.570(13)	0.14465(45)	0 .14465(45)	0.14465(45)	0.575(89)

Goodness of Fit parameters, WRp = 0.0232, Rp = 0.0374, χ^2 = 1.472

The large temperature factor of the 4b site, suggests that this might be a mixed Na-Sr site which, would be be physically plausible. However we were not able to achieve convergence by setting low levels of Na on this site.

S6.3: Thermodiffractometry

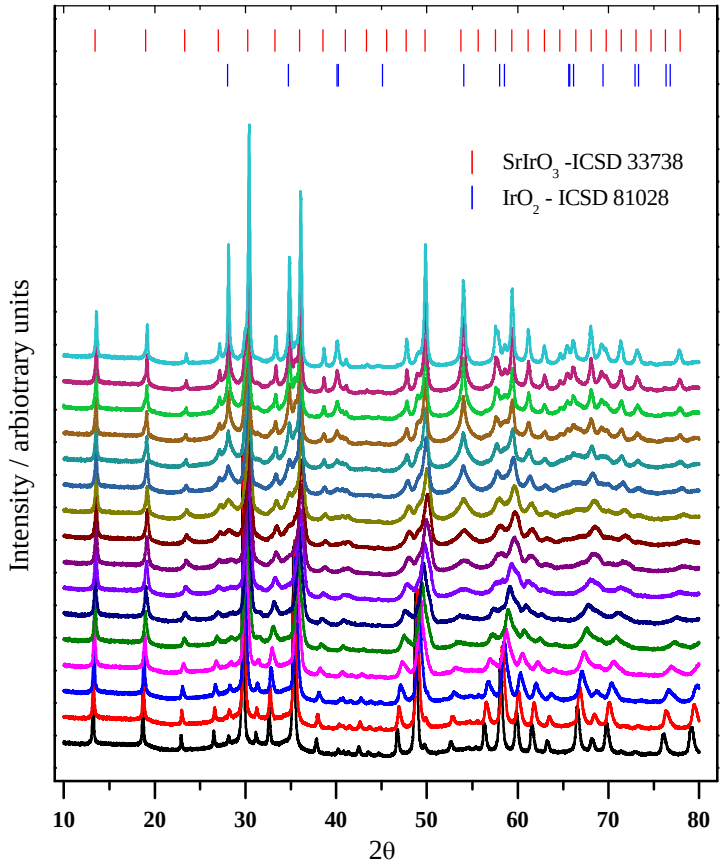

Figure S6.1: *In situ* XRD patterns of $Na_{0.8}Sr_{2.2}Ir_3O_{10.1}$ recorded between 50- 800 ^oC with an interval of 50 ^oC during heating in air . Diffraction patterns are offset for clarity At 450 ^oC, reflections in space groupPn-3 starts disappearing along with the appearance of Bragg peaks of IrO_2. The material above 450 ^oC can be identified as a mixture of IrO_2 and bodycentered $SrIrO_3$: this phase mixture remains stable up to 800 ^oC.

S7 $(Na_{0.27}Ca_{0.59})_2Ir_2O_6.0.66H_2O$

S7.1: Synthesis

$Ca(NO_3)_2.4H_2O$ and $IrCl_3.5H_2O$ were added in a 1:1 molar ratio (0.6 mmole of Ir) to 8 ml of 10 M NaOH solution in a 20 ml Telfon container 4 molar equivalents of solid Na_2O_2 were added as

oxidant before sealing the homogeneous mixture in a stainless-steel autoclave placing in pre-heated oven at 240 ^{o}C for a period of 96 hours. (Alternatively, 50 molar equivalents of H_2O_2 can be used to give the same product.) The black solid product was isolated by suction filtration after cooling and thoroughly washed with deionised water followed by dilute HCl (to remove any $Sr(OH)_2$) and then a final water washing and then dried at 80 ^{o}C in air before further study.

S7.2 Structure refinement

Powder XRD data from the new phase could readily be indexed as a face-centred cubic pyrochlore with a ~ 10.25 Å. Powder neutron diffraction, measured using the POLARIS diffractometer at ISIS, the UK neutron source, was used for structure refinement. Initially the standard pyrochlore structural model was used, and it was found that to match peak intensities, sodium as well as calcium must be present on the A site. Since thermogravimetric analysis indicated the presence of crystal water, the 8b oxygen was modelled as belonging to a water molecule, with proton positions were added on 32e sites at ~1 Å from the 8 b oxygens, based on a model using by Dickens and Weller for hydrated tantalate pyrochlore.[9] Refinement of occupancies of the A site metals along with the 8b oxygens and their associated H atoms gave an excellent fit to the data and a final refined composition of $(Na_{0.27}Ca_{0.59})_2Ir_2O_6.0.66H_2O$. This suggests the presence of iridium in average oxidation state of 4.55, which is consistent with the measure XANES spectra (see main text).

Table S7.1: Crystal structure parameters for $(Na_{0.27}Ca_{0.59})_2Ir_2O_6.0.66H_2O$

Space group $\boldsymbol{Fd\bar{3}m}$, a = 10.25894(11) Å, V = 1079.710(20)Å^3

Atom Site	Wyck.	S.O.F.	x	y	z	U [Å^2] ×100
Ca1	16d	0.587(6)	1/2	1/2	1/2	1.16(6)
Na1	16d	0.273(30)	1/2	1/2	1/2	16.0(18)
Ir1	16c	1	0	0	0	1.234(15)
O1	48f	1	0.32616(9)	1/8	1/8	1.307(13)
O2	8b	0.662(11)	3/8	3/8	3/8	*
H1	32e	0.344(23)	0.3289(4)	0.3289(4)	0.3289(4)	**

Goodness of Fit parameters, WRp = 0.0081, Rp = 0.0121, χ^2 = 2.57 , anisotropic thermal parameters (X100) are, * U_{11} = 2.444(79), U_{22} = 2.44(8) U_{33} = 2.44(8) and ** U_{11} = 75.0(27), U_{22} = 28.4(27) , U_{33} = 75.0(27) U_{12} = -25.0(15), U_{13} = -40.0(15), U_{23}= -25.0(15)

S7.3: TGA

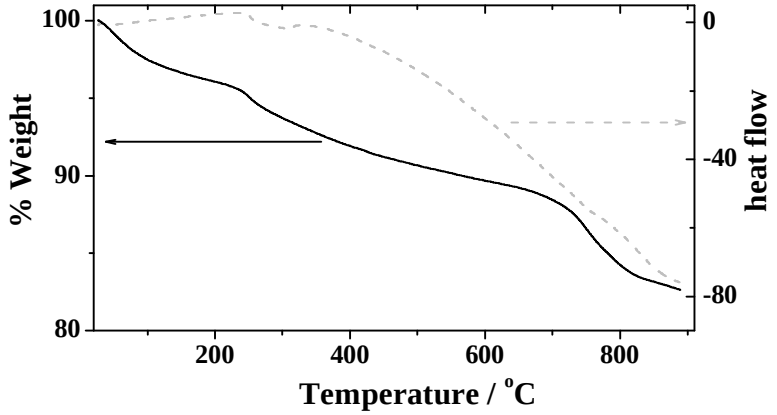

Figure S7.1: TGA/DTA of $(Na_{0.27}Ca_{0.59})_2Ir_2O_6.0.66H_2O$

TGA shows a ~ 2.5 % mass loss from room temperature to 200 °C which is entirely consistent with the loss of crystal water from the refined neutron diffraction composition of $(Na_{0.27}Ca_{0.59})_2Ir_2O_6.0.66H_2O$ (expected 2.16 %), given that a small amount of surface water will inevitably also be present. TGA of other hydrated pyrochlores shows mass losses over similar temperatures, for example, in osmates[10] and tungstates.[11] Continued heating gives further mass loss to ~ 700 °C, associated with collapse and phase separation of the material and the abrupt loss after this is presumably due to the reduction of oxide products to the iridium metal seen in post-heating XRD, Figure S7.2.

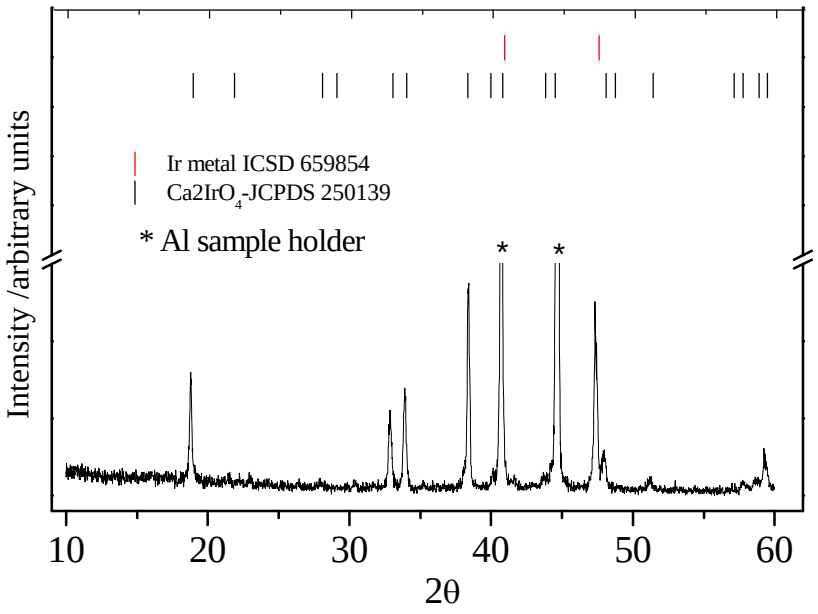

Figure S7.2: PXRD pattern of Ca-Ir-pyrochlore sample heated to 800 °C in air showing formation of a mixture of Ir metal and Ca_2IrO_4

S8: XANES spectroscopy

Figure 8.1 shows the raw, normalised XANES spectra. The second derivative spectra in the main text were used following the method of Choy *et al.* to determine oxidation state.[12] Thus the edge position was defined as the minimum in the second derivative spectrum in the case where a single feature was seen (where the e_g and t_{2g} valence levels are not resolved).

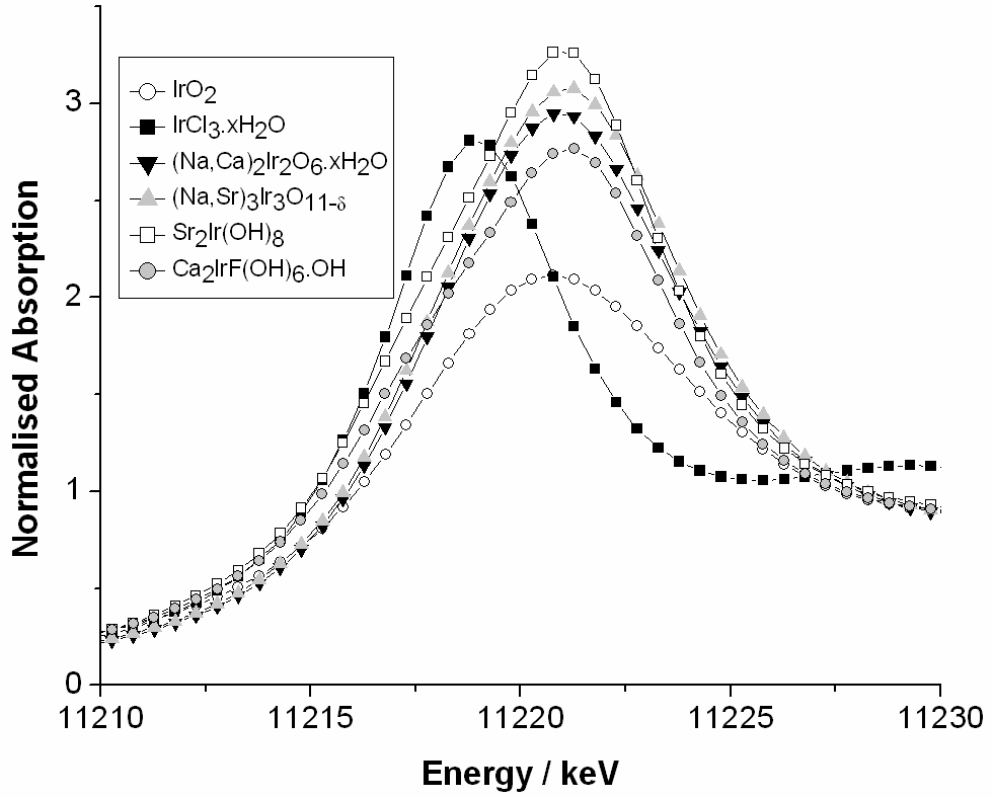

Figure S8.1: Normalised Ir L_{III}-edge XANES spectra of iridium materials and reference compounds.

References for Supporting Information

[1] A. C. Larson and R. B. V. Dreele, *General Structure Analysis System (GSAS)*, **Los Alamos National Laboratory Report LAUR 86-748, 1994**.
[2] G. M. Sheldrick, *Acta Crystallogr. A* **2008**, *64*, 112.
[3] A. S. Wills, *Valist: deposited at www.ccp14.dl.ac.uk*, **1999**.
[4] G. Bandel, C. Platte and M. Trömel, *Z. Anorg. Allg. Chem.* **1981**, *477*, 178-182.
[5] M. M. Wu, X. L. Li, G. P. Shen, J. Li, R. R. Xu and D. M. Proserpio, *J. Solid State Chem.* **2000**, *151*, 56-60.
[6] T. G. Balicheva and N. I. Roi, *Zhurnal Strukturnoi Khimii* **1971.**, *12*, 415
[7] F. Abraham, J. Trehoux and D. Thomas, *J. Less-Common Metals* **1979**, *63*, P57-P63.
[8] H. Watelet, J. P. Picard, J. P. Besse, G. Baud and R. Chevalier, *Solid State Ionics* **1981**, *2*, 191-194.
[9] P. G. Dickens and M. T. Weller, *Solid State Commun.* **1986**, *59*, 569.

[10] R. Galati, C. Simon, C. S. Knee, P. F. Henry, B. D. Rainford and M. T. Weller, *Chem. Mat.* **2008**, *20*, 1652-1659.
[11] G. Rodriguez-Gattorno, L. F. del Castillo and E. Torres-Garcia, *Thermochim. Acta* **2005**, *435*, 176-180.
[12] a) J. H. Choy, D. K. Kim, G. Demazeau and D. Y. Jung, *J. Phys. Chem.* **1994**, *98*, 6258-6262; b) J. H. Choy, D. K. Kim, S. H. Hwang, G. Demazeau and D. Y. Jung, *J. Am. Chem. Soc.* **1995**, *117*, 8557-8566.